2022 IEEE 5th International Conference on Soft Robotics (RoboSoft)
April 4-8, 2022, Edinburgh, UK

A Self-sensing Inverse Pneumatic Artificial Muscle*

Lucrezia Lorenzon[1,2], Giulia Beccali[1,2], Martina Maselli[1,2] and Matteo Cianchetti[1,2], *Member*, *IEEE*

***Abstract*— In recent years, the inverse pneumatic artificial muscles attained great attention in soft robotics, especially for the wider motion range compared to traditional positive pneumatic actuators. Besides self-sensing is a recognized highly desirable property for soft actuators to enable proprioception and to facilitate the soft robots control, a self-sensing strategy for a soft inverse pneumatic muscle was still missing. In this paper, we present the first self-sensing inverse pneumatic artificial muscle in which the reinforcing but compliant element that guides the actuator motion during actuation has not only a mechanical function but, being also electrically conductive, it endows the actuator with self-sensing. Here, the actuator design and manufacturing are described, together with an electro-mechanical characterization. In addition, we demonstrate its self-sensing capability in a dynamic setting, by predicting the actuator strain from its electric resistance variation, through a calibration model.**

I. INTRODUCTION

In the last decades, many research efforts in soft robotics were focused on the development of soft pneumatic actuators to enable wider motion and force capabilities [1], increase the actuators reliability, and introduce novel strategies of sensorization and control. To guide the motion of soft pneumatic actuators, the introduction of material anisotropy through fibers and braided meshes or fabrics have been widely explored [2]. Several actuator designs were investigated and a classification framework based on their operation principle was recently proposed [3]. In general, soft pneumatic actuators are driven through positive pressure or vacuum. Each class of actuators has its strengths and limitations, but in terms of maximum capability of contraction/extension, fluidic actuators based on positive pressures show larger stroke values, especially in elongation, going even beyond 200% of strain [4]. This kind of pneumatic actuator lengthen when pressurized, and it can be used to exert a pulling force during its contraction phase, which is concurrent to a decrease of the actuator internal pressure [5]. In other words, these actuators can be designed to exploit the deflation phase to produce force. Due to this inverted approach with respect to traditional Pneumatic Artificial Muscles (PAMs), they have been recently named Inverted PAMs (IPAMs) [6].

The deformable and compliant nature of soft actuators makes their modelling and control challenging [7]. Several sensorization strategies were proposed, mainly relying on the use of resistive, optical and magnetic principles [8]. Sensing elements introduced to control a soft system should have high accuracy and reliability, while being fully integrated in the soft structure without affecting motion performances. Difficulties in miniaturization and integration of sensors in soft robots made proprioception and self-sensing very ambitious and still poorly achieved in the soft robotics field [7]. In the self-sensing scheme, the actuator deformation is continuously estimated from an inherent property of the actuator itself, thus resulting in a very compact system [9]. Very recently, Bombara et al. developed a self-sensing Twisted-String Actuator (TSA) by replacing one of its mechanical parts with conductive nylon strings and estimating the TSA strain from an electrical signal variation [10], allowing integration and small-scale.

Wakimoto et al., presented a sensorized McKibben actuator in which a conductive rubber strip was integrated in the pneumatic chamber to sense the actuator deformation [11]. In this work, it was demonstrated that a rotational robot arm system that integrates two sensorized McKibben actuators can be accurately controlled without additional external sensors. Liquid metals (e.g. EGaIn) represent a different approach to sense soft actuator deformation [12] and force [13]. This material can be encapsulated into soft channels disposed longitudinally, circumferentially [14] or helically [15] around the actuator body. Other sensorization strategies based on piezoresistive [16], dielectric [17], [18] and optical [19] principles were investigated, but still relying on the attachment of the sensor to the soft actuator, thus with limited integration features. The goal of creating a self-sensing McKibben actuator was pursued by replacing some of the fibers constituting the braided mesh with electrically conductive insulated wires [20], [21]. No additional sensor elements were added to the actuator structure and the braided mesh itself became functional for both the actuator's mechanics and sensing, by exploiting a relation between braid deformation and inductance variation.

In 2018, Yuen et al. presented a fiber-reinforced bending and extending fascicle of artificial muscles in which capacitive soft sensors were embedded in the inner surface of the pneumatic chambers [22]. A self-sensing extensible pneumatic actuator was proposed by Azami et al. [23]. The actuator was made by surrounding a cylindrical elastomeric chamber with a metal spring, whose purpose was to restrain the chamber radial expansion during pressurization but also to measure the displacement from the change in inductance with the length. However, besides efforts were later made to integrate the spring in the actuator soft body [24], the

*This work was partially supported by the European Commission through the Hybrid Heart Project under Grant 767195.

[1]Lucrezia Lorenzon (corresponding author), Giulia Beccali, Martina Maselli and Matteo Cianchetti are with The BioRobotics Institute, Scuola Superiore Sant'Anna, Pisa, Italy. lucrezia.lorenzon, giulia.beccali, martina.maselli, matteo.cianchetti@santannapisa.it

[2]Department of Excellence in Robotics & AI, Scuola Superiore Sant'Anna, Pisa, Italy.

2022 IEEE 5th International Conference on Soft Robotics (RoboSoft) | 978-1-6654-0828-8/22/$31.00 ©2022 IEEE | DOI: 10.1109/ROBOSOFT54090.2022.9762204

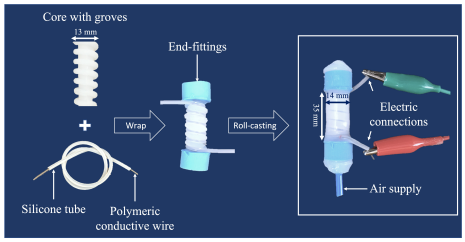

Fig. 1. Fabrication process and final self-sensing IPAM prototype (right).

employed spring is a stiffer element whose long-term interaction with the silicone could lead to failure and should be investigated.

To the best of our knowledge, this paper is the first study on a self-sensing IPAM that relies on a piezoresistive principle and that is totally soft. We realized the self-sensing capability of the IPAM through the integration of a stretchable polymeric and electrically conductive wire, arranged in a helical configuration and totally embedded in the actuator elastomeric body. The novelty is represented by the exploitation of the twofold functionality of the soft helical structure. It has not only the mechanical function of guiding the actuator deformation along its longitudinal axis, but it can be used to sense the actuator variations in length through electrical resistance changes. Indeed, the electrical resistance of the employed polymeric wire increases when it is stretched. Thus, the integration of this wire into the IPAM allows the sensing of the actuator deformation by measuring the wire electrical resistance variation. In this paper, we describe a simple fabrication process to realize a self-sensing IPAM in a few steps. The results of the characterization experiments performed both on the polymeric wire itself and on the actuator are presented, together with a calibration model that allowed the prediction of the self-sensing IPAM strain during dynamic testing.

II. MATERIALS AND METHODS

A. Self-sensing IPAM design and manufacturing

The developed self-sensing IPAM is based on a hollow cylindrical body, constituting the pneumatic chamber of the actuator. In the actuator body, the elastomeric matrix hosts the helical structure with a twofold function: when a positive pressure is applied on the pneumatic chamber, the helical structure constrains the actuator radial expansion and drives the deformation along its principal axis, causing pure elongation. Concurrently, it gives electrical feedback, endowing the IPAM with a self-sensing capability.

The helical structure is made of a polymeric conductive wire whose external diameter is 1 mm and a coaxial silicone hollow tube with a 1.2 mm internal diameter and external diameter d_e = 2.6 mm (Stonfo ITALY). The conductive wire is a commercial product designed for high-performance shielding, mainly for military applications (Holland Shielding System BV [25]). The selected wire is a solid silicone cord doped with carbon or silver particles that make it electrically conductive. We preliminary observed that the direct contact between the conductive wire and the uncured silicone is a cause of loss of conductive properties. Thus, to limit the interaction between wire and uncured silicone, the commercial hollow tube made of silicone was introduced.

Particular attention was given to the choice of the silicone matrix, in combination with the selection of the most suitable conductive wire. For the silicone matrix, Ecoflex 50, EF50 (Smooth-On, Inc.) and DragonSkin 10 Slow, DS10 (Smooth-On, Inc.) were evaluated, and both carbon-based and silver-based conductive wires were considered. Three samples per matrix and wire materials combination were fabricated and tested. Each sample is a silicone cylinder of length 70 mm in which a piece of 80 mm long conductive wire passed through the silicone tube, is embedded. As references, we also used the wire alone, and the wire inserted in the silicone tube, but not embedded in any matrix. The value of electrical resistance between the extremities of the wire was collected using a multimeter, at regular intervals: immediately after the end of the silicone curing (day 0), and in the following four days, every 24h. The selection of the most performing combination of elastomeric matrix and conductive wire materials was based on the ability of the wire to maintain its electrical conductivity in time.

The helix must have a constant pitch and be embedded in the elastomeric matrix [26]. This avoids any sliding or relative displacement of the helical structure with respect to the actuator body during actuation, which would lead to the actuator failure due to ballooning [22]. Thus, for the self-sensing IPAM fabrication, a first core structure with a 2 mm internal diameter was made by casting silicone in a 3D-printed mold. The external surface presents helical groves whose pitch is $2 * d_e = 5.2$ mm to guide the winding of the silicone tube with the conductive wire (see Fig. 1). Then, the roll-casting technique was used to create an external uniform silicone surface to embed the helical structure.

Two end-fittings were realized at the actuator edges by casting Smooth-Sil 950 (Smooth-on, Inc.), a stiffer silicone with respect to EF50 and DS10, which provides perfect sealing, stable fixing points and an easy coupling with the air supply. Finally, silicone glue (Sil-Poxy, Smooth-on, Inc.) was used to assure air tightness.

B. Sensor characterization

The wire used in this work is a silicone-based solid cord with addition of particles of carbon, that make the wire electrically conductive.

The electro-mechanical characterization of the wire was conducted with the universal testing machine (Instron Inc., Norwood, MA) in displacement control mode. Firstly, tensile tests were carried out to evaluate its elastic modulus. Three samples of length 20 mm were tested until rupture at velocity 50 mm/min.

In addition, considered that the piezoelectric helical structure is arranged along the actuator axial direction, we expect that the conductive wire is subject to small tensile deformations, thus a very sensitive sensor element is required. For this reason, a preliminary experiment was conducted to

assess if a resistance variation of the wire can be recorded in response to a small stretch. Thus, a sample of length 15 mm was tested over five loading and unloading cycles on a strain range 0-2.5% and at 1 and 5 mm/min. While the testing machine applied a controlled strain to the sample, the force was recorded and an acquisition circuit was employed to concurrently measure the wire variations in electrical resistance. Each end of the wire was clamped by the testing machine grippers and connected to the electric circuit through copper sheets. The electric circuit is a voltage divider in which the variable resistance R_V (represented by the wire) is connected in series with a constant resistance $R_C = 119.6\ \Omega$. The two resistances are connected at the positive input terminal of an operational amplifier and the voltage supply $V_{in} = 5\ V$ is applied at the ends of the series. The negative input terminal of the buffer is connected to the ground and the output voltage V_{out} is recorded at its output terminal. A data acquisition board (DAQ, National Instruments R) powers the circuit and registers the voltage signal at 50 Hz. The variable resistance of the wire is calculated from the relationship $V_{out} = R_V V_{in}/(R_V + R_C)$ and it was matched with the strain applied by the testing machine.

C. Electro-mechanical characterization of the IPAM

A mechanical characterization of the self-sensing IPAM is conducted through both a pressure-strain and a force-strain test, as in [4] and [5]. In the pressure-strain experiment, three actuators were statically tested over four loading and unloading pressure cycles ranging from 0 to 1.8 bar, with pressure steps of 0.2 bar. The continuous air supply was provided by a compressor (Fiac Air Compressors, Leonardo) and modulated through an electronic valve (CAMOZZI, K8P-0-D522-08). A digital manometer (CAMOZZI, SWCN-P10-P3-2) was employed to continuously measure the actuator internal pressure. The actuator length was measured at each pressure step with a caliper and the strain was computed as $\epsilon = (L_a - L_0)/L_0$, where L_a is the actual length and L_0 the rest length at pressure P = 0 bar. In the data analysis, the first cycle was excluded to account for the Mullin's effect. We also computed the maximum elongation $\epsilon_e = (L_{max} - L_0)/L_0$ and the maximum contraction $\epsilon_c = (L_0 - L_{max})/L_{max}$, where L_{max} is the maximum achieved actuator length at pressure P = 1.8 bar. The pressure range of this test was selected to explore a sufficiently wide elongation range, while still preserving the actuator functionality over repetitive testing cycles. Indeed, the bursting pressure of the developed self-sensing IPAM was preliminary assessed by pressurizing three actuators in steps of 0.2 bar, until rupture. Three self-sensing IPAM were also characterized in terms of force using a universal testing machine (Instron Inc., Norwood, MA). A cyclic tensile test was conducted over five cycles, applying a 50% maximum strain at 50 mm/min, while the actuator internal pressure was 0 bar. Each test was repeated three times on each of the tested actuators. In the data analysis, the first cycle of each test was excluded.

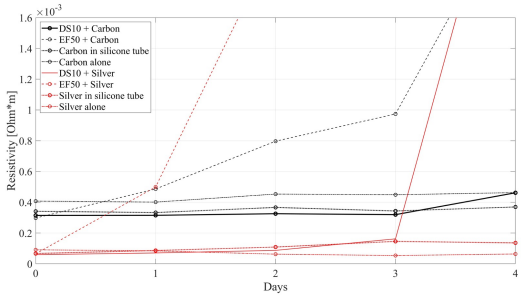

Fig. 2. Carbon/silver-based polymeric wires resistance monitoring over 4 days: wire alone, wire inserted in the silicone tube and wire inserted in the silicone tube and embedded in the elastomeric matrix made of EF50/DS10.

D. Verification of the IPAM capabilities of self-sensing

During the static pressure-strain tests described in section II-C, the acquisition circuit reported in section II-B was used to record the actuator resistance R for 5 s, at each pressure step. The actuator resistance at P = 0 bar is indicated with R_0, and the ratio R/R_0 is related to the actuator strain.

To build a reliable calibration curve for our self-sensing IPAM, the pressure range of interest was restricted on the base of the experimental results, so to have a monotonic loading and unloading curve. The relationship between resistance variation and strain was adjusted accordingly, by considering as initial resistance R_0 and length L_0 the corresponding values measured on the actuator at the lowest pressure value. A very simple single-valued calibration curve is obtained by fitting the experimental data, as a mean between the loading and the unloading curve.

To assess the usability of the developed calibration curve for a prediction of the self-sensing IPAM length through wire electrical resistance, a dynamic test was performed. The actuation pressure of one self-sensing IPAM was varied in step of 0.2 bar between 1.2 and 1.8 bar, over three cycles of increasing and then decreasing pressure. Simultaneously, both the actuator resistance and length were recorded. The real-time measure of the actuator length was obtained from a video analysis (Tracker, physlets.org, Open Source Physics). The accuracy of our model was assessed by calculating the RMSE and the Spearman's correlation coefficient r_s (significance level 0.05) between the actuator strain obtained from a post-processing of the data coming from video analysis and the actuator strain calculated from the resistance measures, by using our model. Also, the absolute error was calculated.

III. RESULTS AND DISCUSSION

A. Wire choice and characterization

The direct comparative analysis between silver based and carbon based wires reveals that the silver based wire lost its electrical conductive properties in a few days after being embedded in either EF50 and DS10, while the resistance of the carbon based wire embedded in the DS10 remains almost constant for the whole time frame of observation, lasted 4 days (Fig. 2). Most probably, the loss of electrical conductivity that was observed is related to the diffusion

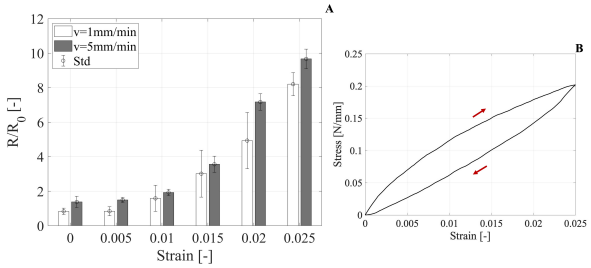

Fig. 3. a) Carbon-based polymeric wire resistance variation with respect to strain, at testing velocity equal to 1 mm/min and 5 mm/min. b) Stress-strain curve at 1 mm/min.

of carbon atoms belonging to the conductive wire. In light of these results, the self-sensing IPAM is fabricated with an elastomeric matrix made of DS10 and a helical structure containing a carbon-based polymeric wire (see Fig. 1).

In addition, the electro-mechanical test results confirm that the carbon-based commercial wire has an electric resistance that varies with its deformation. The bar chart in Fig. 3a shows that the ratio between wire resistance R and its initial value R_0, measured at the beginning of each test, increases both with the applied strain and with the velocity of the test. In the data analysis, the average resistance between loading and unloading of each cycle is calculated. The mean value of R/R_0 between cycles and the standard deviation, at each strain level, are also reported in figure 3a. The ratio R/R_0 at strain equal to zero is 0.83 ± 0.18 and 1.38 ± 0.33, at 1 mm/min and 5 mm/min, respectively. Indeed, we observed a progressive increase of the electric resistance of the wire R with the increasing number of cycles during dynamic testing. At low testing velocity, the conductive wire has time to recover its rest shape and, consequently, its electric properties. At a velocity of 5 mm/min, the resistance of the wire almost doubles at only 1% strain ($R/R_0 = 1.93 \pm 0.19$), while at 2.5% strain it becomes around 10 times ($R/R_0 = 9.67 \pm 0.57$). The variation of the electric resistance in the wire is given by a piezoresistive effect and it is related to the mechanical deformation of the wire. The mechanical deformation is time-dependent and also the electric resistance variation depends on the velocity of the applied strain. The average stress-strain curve between cycles shows elasticity with considerable hysteresis (Fig. 3b).

The mechanical properties of the carbon based wire were investigated with uniaxial tensile tests. The wire elastic modulus, calculated at 10% of strain, results to be 6.2 MPa, a value that is around 40 times the DS10 elastic modulus at 100% of strain provided from the manufacturer (0.15 MPa).

This preliminary investigation on the commercial carbon-based polymeric wire further supported its selection as a helical structure for a self-sensing IPAM. The wire sensibility to stretch is high, and an electrical signal variation is detected even at low strain values. In addition, the stiffness difference between the helical structure and the elastomeric matrix is sufficient to minimize the actuator radial expansion while allowing axial elongation, as desired.

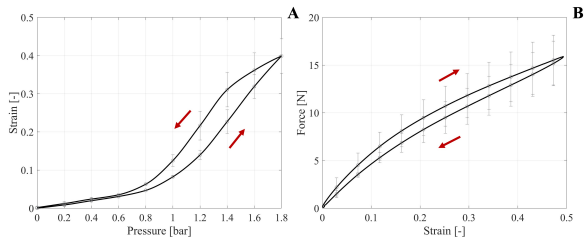

Fig. 4. a) Pressure-strain behaviour of the self-sensing IPAM, over the pressure range P = 0 - 1.8 bar. b) Force-strain behaviour of the self-sensing IPAM, at pressure P = 0 bar.

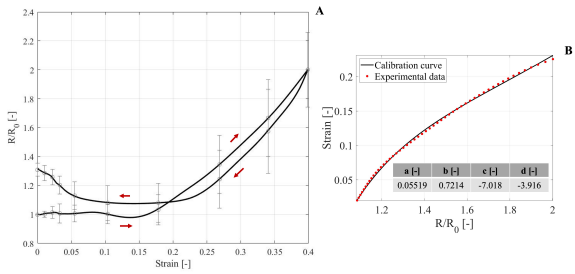

Fig. 5. Self-sensing IPAM relationship between resistance variation and strain: a) the rest values of resistance R_0 and length L_0 are set when the actuating pressure is P = 0 bar; b) calibration curve. The rest value of resistance R_0 and length L_0 are set when the actuating pressure is P = 1.2 bar.

B. Electro-mechanical characterization of the IPAM

The pressure-strain relationship of the self-sensing IPAM is nonlinear and presents hysteresis (see Fig. 4a). At the maximum pressure of 1.8 bar, the average maximum elongation and contraction are 39.9% and 27.4%, respectively. The self-sensing IPAM performances are comparable with previous extensible pneumatic muscles (such as [27]), in terms of stroke. In addition, we observed that, upon pressurization, the actuator elongates and slightly rotates, because of the helical arrangement of the reinforcing structure [28]. The quantification of the rotation angle was considered out of scope for this study.

The maximum force that the inverse actuator can apply, at different strain levels, is shown in Fig. 4b. At 40% of strain, the elastic return force exerted when the internal pressure is 0 bar is 13.6 N, a force value that already demonstrated its suitability for soft robotics applications such as in elbow and knee assistive devices driven by extensible fluidic actuators [29].

C. Verification of the IPAM capabilities of self-sensing

The static calibration tests conducted with the self-sensing IPAM reveal that, in the loading phase, the actuator electrical resistance monotonically increases after 15% of strain, as visible in Fig. 5a. The resistance doubles ($R/R_0 = 2$) when the maximum pressure of 1.8 bar is applied and the actuator strain is 40%. During unloading, the actuator electrical resistance monotonically decreases between 40% and 20% of strain, before intersecting the loading curve, when the actuating pressure is 1.2 bar. At the end of each

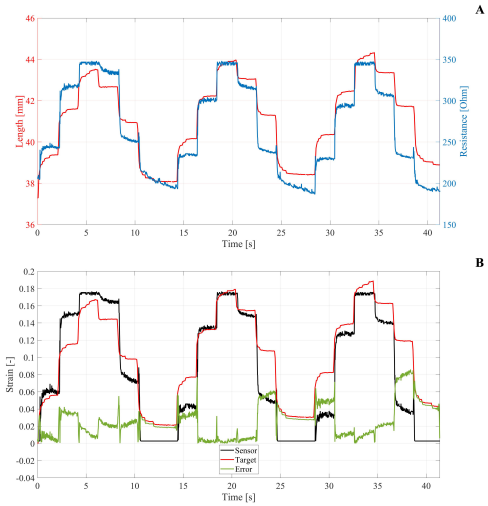

Fig. 6. Self-sensing IPAM dynamic testing over three loading and unloading cycles and actuator strain prediction. a) Self-sensing IPAM nominal resistance and absolute length, with respect to time; b) self-sensing IPAM strain prediction from the calibrated sensor and measured target strain, in time. The time evolution of the absolute error is also reported.

cycle, the resistance R at P = 0 bar is greater than the initial one, in accordance to what observed from the preliminary electro-mechanical tests that were made on the conductive wire (Fig. 3a).

The strong correlation between driving pressure and resistance variation, together with the peculiarities of the resistance-strain characteristic of the self-sensing IPAM, guided the selection of 1.2 - 1.8 bar as the optimal working pressure range for the developed sensorized actuator. Indeed, in this range, the resistance-strain relation is monotonic and no resistance increasing drift was observed. In addition, for the self-sensing IPAM application as a soft actuator, the working range setting is not a limiting factor but a simple procedure to match the actuator stroke with the requirements.

The calibration of the sensor is made by fitting the experimental data with a second-order exponential function (equation 1).

$$\epsilon = a\, e^{b\,\frac{R}{R_0}} + c\, e^{d\,\frac{R}{R_0}} \tag{1}$$

The calibration curve is reported in Fig. 5b, together with the fitting parameters ($R^2 \approx 0.999$).

During dynamic testing of our self-sensing IPAM, the actuator length and resistance were recorded (see Fig. 6a). The actuator electrical resistance is extremely sensitive to the actuator deformation, without delays. Also, under repetitive loading and unloading cycles, the actuator resistance variation is repeatable and with a stable relation with the driving pressure. The variation noticed after several working cycles regards a slight increase of the actuator strain, probably due to a progressive softening of the elastomeric materials that constitute the self-sensing IPAM. Most probably, a preconditioning of the actuator before testing stabilizes the rest length of the actuator at different pressures, and a single valued relation between electric resistance and strain can be found.

When the sensing capability of the self-sensing IPAM is used and our calibration model is applied, the actuator strain is predicted from the electrical resistance readings (Fig. 6b). The RMSE between the measurements obtained from calibrated electrical resistance data and from video analysis is 3.26%, with a good correlation between the two signals ($r_s = 0.92$, $p < 0.05$). The absolute error is reported in figure 6b and calculated as $e(t) = |\epsilon(t) - \hat{\epsilon(t)}|$, where $\epsilon(t)$ and $\hat{\epsilon(t)}$ are the predicted actuator strain from the model (sensor) and the measured strain from video analysis (target), respectively. The average absolute error on the strain is 2.6%. With the increasing number of working cycles, the strain is underestimated by the model. This result is in accordance with our expectations: the self-sensing IPAM calibration was obtained from a quasi-static experiment, thus, it cannot account for the observed increasing drift of the maximum actuator strain over repetitive working cycles. If a dynamic actuation is foreseen, the calibration model should be refined and improved, to also account for additional dynamic factors, such as the inflation rate. The 2.6% error on the strain corresponds to 0.97 mm error on the actuator length, if calculated with respect to 37.3 mm, that is the tested actuator length at pressure 1.2 bar. This error is not negligible for applications that need high precision, but still, the proposed solution is very advantageous for monitoring actuator functioning through self-sensing properties, without the need of additional sensing elements. The precision that we obtain in the prediction of the actuator strain is in line with previous works on sensorized positive pneumatic actuators [16], [20]. Relatively to the inverse pneumatic actuators, the sensing presented in [23] and [24] is more accurate, but it is based on the inductance variation principle of a rigid constituting element of the actuator.

IV. CONCLUSIONS AND FUTURE WORK

In this paper, we present the first study on a self-sensing inverse pneumatic artificial muscle. We introduce a compliant and electrically conductive helical reinforcing structure to both guide the actuator deformation and give an electrical feedback during operation, thus endowing the actuator with a self-sensing capability.

The electro-mechanical characterization of the developed self-sensing IPAM reveals that, at the maximum actuating pressure of 1.8 bar, the actuator elongates by 40% and its electrical resistance doubles. Being designed as an inverse actuator, the maximum pulling force of over 13 N is exerted at its maximum elongation and when the internal pressure is set to 0 bar. The mechanical performances in terms of both stroke and force are in the range of state-of-art pneumatic actuators. Thus, its intrinsic additional self-sensing capability makes our self-sensing IPAM a good alternative candidate for actuation systems in several soft robotics applications. We demonstrated that the actuator strain can be predicted from the electrical resistance variation, with a 2.6% average absolute error on the predicted strain. Indeed, during actuation, the piezoelectric helical structure is deformed by the radial pressure and a relation between pneumatic pressure

and electrical resistance is obtained. During dynamic testing, a increasing drift of the actuator length over time is observed, and our calibration model slightly underestimates the actuator deformation. To reduce this error, the sensor calibration could be performed on preconditioned actuators, that underwent several preliminary working cycles to stabilize their mechanical properties, thus the actuator length in relation to the applied internal pressure. However, the focus of this paper is the development of a novel self sensing strategy for a IPAM, and the optimization of the actuator reliability itself will be subject of future studies.

The experimental tests show that, thanks to the complete embedding of the designed helical structure and the material compatibility with the elastomeric matrix, the actuator works without ballooning issues, often recognised as the major cause of failure for fiber-reinforced fluidic actuators [22]. Further studies on the constituting materials and the adopted manufacturing procedure could even widen the self-sensing IPAM range of stroke and pulling force. Also, the long-term stability of the conductive properties of the carbon-based polymeric wire embedded in the DS10 matrix should be deeper investigated.

In conclusion, the developed self-sensing IPAM is composed of soft materials and compliant elements only and possesses intrinsic self-sensing capabilities. Thanks to its uniform elastomeric surface, its integration in a complex soft system is straightforward, enabling proprioception and closed-loop control.

REFERENCES

[1] J. Bishop-Moser, G. Krishnan, C. Kim, and S. Kota, "Design of soft robotic actuators using fluid-filled fiber-reinforced elastomeric enclosures in parallel combinations," in *2012 IEEE/RSJ International Conference on Intelligent Robots and Systems*, pp. 4264–4269, IEEE, 2012.

[2] M. Zhu, T. N. Do, E. Hawkes, and Y. Visell, "Fluidic fabric muscle sheets for wearable and soft robotics," *Soft robotics*, vol. 7, no. 2, pp. 179–197, 2020.

[3] H. D. Yang, B. T. Greczek, and A. T. Asbeck, "Modeling and analysis of a high-displacement pneumatic artificial muscle with integrated sensing," *Frontiers in Robotics and AI*, vol. 5, p. 136, 2019.

[4] L. Lorenzon, D. Zrinscak, M. Maselli, and M. Cianchetti, "Modelling and characterization of a soft inverse pneumatic artificial muscle," in *ACTUATOR; International Conference and Exhibition on New Actuator Systems and Applications 2021*, pp. 1–4, VDE, 2021.

[5] T. Yukisawa, Y. Ishii, S. Nishikawa, R. Niiyama, and Y. Kuniyoshi, "Modeling of extensible pneumatic actuator with bellows (epab) for continuum arm," in *2017 IEEE International Conference on Robotics and Biomimetics (ROBIO)*, pp. 2303–2308, IEEE, 2017.

[6] E. W. Hawkes, D. L. Christensen, and A. M. Okamura, "Design and implementation of a 300% strain soft artificial muscle," in *2016 IEEE International Conference on Robotics and Automation (ICRA)*, pp. 4022–4029, IEEE, 2016.

[7] N. Farrow, Y. Li, and N. Correll, "Morphological and embedded computation in a self-contained soft robotic hand," *arXiv preprint arXiv:1605.00354*, 2016.

[8] J. Walker, T. Zidek, C. Harbel, S. Yoon, F. S. Strickland, S. Kumar, and M. Shin, "Soft robotics: a review of recent developments of pneumatic soft actuators," in *Actuators*, vol. 9, p. 3, Multidisciplinary Digital Publishing Institute, 2020.

[9] D. Bombara, R. Konda, and J. Zhang, "Experimental characterization and modeling of the self-sensing property in compliant twisted string actuators," *IEEE Robotics and Automation Letters*, vol. 6, no. 2, pp. 974–981, 2021.

[10] D. Bombara, V. Mansurov, R. Konda, S. Fowzer, and J. Zhang, "Self-sensing for twisted string actuators using conductive supercoiled polymers," in *Smart Materials, Adaptive Structures and Intelligent Systems*, vol. 59131, p. V001T04A009, American Society of Mechanical Engineers, 2019.

[11] S. Wakimoto, K. Suzumori, and T. Kanda, "Development of intelligent mckibben actuator," in *2005 IEEE/RSJ International Conference on Intelligent Robots and Systems*, pp. 487–492, IEEE, 2005.

[12] L. O. Tiziani, T. W. Cahoon, and F. L. Hammond, "Sensorized pneumatic muscle for force and stiffness control," in *2017 IEEE International Conference on Robotics and Automation (ICRA)*, pp. 5545–5552, IEEE, 2017.

[13] J. Wirekoh, L. Valle, N. Pol, and Y.-L. Park, "Sensorized, flat, pneumatic artificial muscle embedded with biomimetic microfluidic sensors for proprioceptive feedback," *Soft robotics*, vol. 6, no. 6, pp. 768–777, 2019.

[14] D. Sarkar, S. Pal, S. S. Roy, A. Kumar, and A. Arora, "Estimation of transmission force in assistive devices using conductive liquid metal based sensorized pneumatic artificial muscle," in *2020 5th IEEE International Conference on Recent Advances and Innovations in Engineering (ICRAIE)*, pp. 1–5, IEEE, 2020.

[15] Y.-L. Park and R. J. Wood, "Smart pneumatic artificial muscle actuator with embedded microfluidic sensing," in *SENSORS, 2013 IEEE*, pp. 1–4, IEEE, 2013.

[16] M. Maselli, D. Zrinscak, V. Magliola, and M. Cianchetti, "A piezoresistive flexible sensor to detect soft actuator deformation," in *2019 2nd IEEE International Conference on Soft Robotics (RoboSoft)*, pp. 372–377, IEEE, 2019.

[17] N. Goulbourne and S. Son, "Numerical and experimental analysis of mckibben actuators and dielectric elastomer sensors," in *ASME International Mechanical Engineering Congress and Exposition*, vol. 43041, pp. 175–185, 2007.

[18] R. Kanno, S. Watanabe, K. Shimizu, and J. Shintake, "Self-sensing mckibben artificial muscles embedded with dielectric elastomer sensor," *IEEE Robotics and Automation Letters*, vol. 6, no. 4, pp. 6274–6280, 2021.

[19] B. Jamil and Y. Choi, "Modified stiffness based soft optical waveguide integrated pneumatic artificial muscle (pam) actuators for contraction and force sensing," *IEEE/ASME Transactions on Mechatronics*, 2021.

[20] W. Felt, K. Y. Chin, and C. D. Remy, "Contraction sensing with smart braid mckibben muscles," *IEEE/ASME Transactions on Mechatronics*, vol. 21, no. 3, pp. 1201–1209, 2015.

[21] W. Felt, S. Lu, and C. D. Remy, "Modeling and design of "smart braid" inductance sensors for fiber-reinforced elastomeric enclosures," *IEEE Sensors Journal*, vol. 18, no. 7, pp. 2827–2835, 2018.

[22] M. C. Yuen, R. Kramer-Bottiglio, and J. Paik, "Strain sensor-embedded soft pneumatic actuators for extension and bending feedback," in *2018 IEEE International Conference on Soft Robotics (RoboSoft)*, pp. 202–207, IEEE, 2018.

[23] O. Azami, D. Morisaki, T. Miyazaki, T. Kanno, and K. Kawashima, "Development of the extension type pneumatic soft actuator with built-in displacement sensor," *Sensors and Actuators A: Physical*, vol. 300, p. 111623, 2019.

[24] O. Azami, T. Kawase, T. Miyazaki, T. Kanno, and K. Kawashima, "External force estimation of pneumatic soft actuator with built-in displacement sensor," *Sensors and Materials*, vol. 33, no. 2, pp. 555–567, 2021.

[25] Holland Shielding Systems BV, Conductive rubber O-profiles 7900, https://hollandshielding.com/Conductive-rubber-O-Profiles, accessed 18-02-2022.

[26] E. H. Skorina, M. Luo, W. Y. Oo, W. Tao, F. Chen, S. Youssefian, N. Rahbar, and C. D. Onal, "Reverse pneumatic artificial muscles (rpams): Modeling, integration, and control," *PloS one*, vol. 13, no. 10, p. e0204637, 2018.

[27] L. Guo, K. Li, G. Cheng, Z. Zhang, C. Xu, and J. Ding, "Design and experiments of pneumatic soft actuators," *Robotica*, vol. 39, no. 10, pp. 1806–1815, 2021.

[28] F. Connolly, P. Polygerinos, C. J. Walsh, and K. Bertoldi, "Mechanical programming of soft actuators by varying fiber angle," *Soft Robotics*, vol. 2, no. 1, pp. 26–32, 2015.

[29] S. Sridar, C. J. Majeika, P. Schaffer, M. Bowers, S. Ueda, A. J. Barth, J. L. Sorrells, J. T. Wu, T. R. Hunt, and M. Popovic, "Hydro muscle-a novel soft fluidic actuator," in *2016 IEEE International Conference on Robotics and Automation (ICRA)*, pp. 4014–4021, IEEE, 2016.